Tunable metasurface external-cavity quantum cascade lasers up to 5.74 THz

Mohammad Shahili, ‡ Anthony D. Kim, ‡ Sadhvikas J. Addamane, Christopher A. Curwen, Jonathan H. Kawamura, Benjamin S. Williams*

Mohammad Shahili and Anthony D. Kim − Department of Electrical and Computer Engineering, University of California, Los Angeles, CA 90095, USA, E-mail: mshahili0@g.ucla.edu.

Sadhvikas J. Addamane − Sandia National Laboratories, Center of Integrated Nanotechnologies, MS 1303, Albuquerque, NM 87185, USA

Christopher A. Curwen and Jonathan H. Kawamura − Jet Propulsion Laboratory, California Institute of Technology, Pasadena, CA 91109, USA

Benjamin S. Williams − Department of Electrical and Computer Engineering, University of California, Los Angeles, CA 90095, USA

ABSTRACT:

Vertical-external-cavity surface-emitting-lasers based upon amplifying quantum-cascade metasurfaces are demonstrated in the 5–6 THz range for the first time. Enhanced parasitic coupling to lossy surface modes requires updated design guidelines, while elevated losses and lower available material gain limit the scaling of the metasurface period from previous designs. A series of metasurface devices with varying periods employing both uniform and focusing metasurfaces is fabricated and characterized. Reducing the metasurface period below 70% of the free-space wavelength enables devices with superior performance, achieving pulsed operation up to 5.74 THz with peak output powers of 1.3 mW, maximum operating temperatures up to 83 K, and continuous-wave operation up to 54 K with 23 μW of output power. In the best case, single-mode tuning from 5.23–5.73 THz, which corresponds to a 9.1% fractional tuning, is realized with near-Gaussian far-field profiles maintained across the entire range. These results establish quantum cascade vertical-external-cavity surface-emitting-lasers as promising candidates for high-frequency local oscillator applications in heterodyne spectroscopy.

KEYWORDS: quantum cascade laser; vertical-external-cavity surface-emitting-laser; terahertz; *Reststrahlen* band; gallium arsenide;

INTRODUCTION:

High-resolution heterodyne receivers in the terahertz spectral range have found significant application in astrophysics, space, and atmospheric science. For example, they can spectrally resolve the complicated Doppler-limited lineshapes of various molecular and atomic species in the interstellar medium. One of the essential components of a heterodyne receiver is a stable local oscillator (LO) with sufficient power to pump the mixers of choice. Quantum cascade lasers (QCLs) have emerged as viable LO candidates in the 3–5 THz range, where the efficiency of Schottky-diode frequency-multiplier chains decreases.[1] QC-lasers have been used in three recent heterodyne instruments — upGREAT on the SOFIA airborne observatory, and the balloon-based GUSTO and OSAS-B — all targeting the 4.74 THz neutral oxygen [OI] line.[2–4] The next technological challenge is to push QC-laser LOs above 5 THz—a frequency region containing astrophysically important lines such as [NIII] (5.23 THz), [SI] (5.32 THz), [FeI] (5.52 THz), [OIII] (5.79 THz), and [FeIII] (5.8 THz).[5]

Despite this growing interest, making an efficient QCL above 5 THz faces fundamental challenges.[6] The root cause of the difficulty is the energetic proximity of photon to the optical phonon branches in gallium arsenide (GaAs); the transverse optical phonon has a frequency of 8.1 THz and the longitudinal optical phonon frequency is 8.8 THz. The first issue is the strong optical loss in the semiconductor for frequencies near the polar optical phonon frequencies.[7] Although not as fundamental, there are also worsening losses originating from the heavily doped n^+ GaAs material typically used as part of the electrical contact. The second issue is the reduced population inversion and gain. QC active regions designed for higher frequency operation require larger energy separations between the upper and lower radiative states. This reduces the activation energy required for electrons in the upper state to emit a longitudinal optical phonon, which leads to exponentially faster thermally activated non-radiative scattering, degradation of population inversion, and residual ISB absorption of electrons in the ground state.

Consequently, there have been few reports of QCLs operating above 5 THz. Early reports were limited to 5.4 THz and below, and had operating temperatures no higher than ~55 K in pulsed mode;[6] CW operation was not reported above 15 K, if at all.[8] More recently a new generation of optimized active region and waveguide designs has pushed coverage as high as 6 THz, with maximum pulsed mode operating temperatures of 117 K; CW operation at 5.71 THz was observed up to 68 K.[9] However, these results were obtained in multimoded metal-metal ridge waveguide Fabry-Pérot cavities without any effort made toward beam pattern or precise frequency control. While these devices serve as proof that active regions can provide gain in the 5–6 THz range, they are not yet practical for local oscillators or other spectroscopic instruments.

A compelling approach for a practical device is the quantum-cascade vertical-external-cavity surface-emitting laser (QC-VECSEL) architecture, in which an reflectarray metasurface is loaded with QC gain material to provide amplification, and is paired with a partially transmissive output coupler to create the optical cavity.[10] In diverse implementations, the VECSEL architecture supports peak powers from milliwatt up to watt-level, near-diffraction-limited Gaussian beams, broad wavelength tunability, and suitability for phase- and injection-locking.[11–15] QC-VECSELs have already been demonstrated in the 1.76–4.9 THz range, and offer scalability and mode control that are difficult to achieve with conventional QCL designs.

In this work, we present the first realization of a QC-VECSEL operating above 5 THz. At these frequencies, we show that the increased losses and reduced availability of gain constrains the metasurface and VECSEL design space. In particular, it is found to be critical to properly choose the metasurface period to avoid coupling to lossy Bragg modes. A series of metasurface QC-lasers are fabricated and experimentally validated against finite element method (FEM) simulations.

METHODS:

The QC-VECSEL cavity comprises an amplifying metasurface and a highly reflective output coupler. The active metasurface consists of a subwavelength-periodic array of microcavity metal-

metal waveguide ridge antennas loaded with THz QC gain material. The output coupler is fabricated using evaporated gold circular mesh on ~100 μm-thick quartz substrates, with simulated reflectance ranging from 0.97 to >0.99. More detail on the output coupler is given in the Supporting Information. Figure 1a shows an SEM image of the metasurface and the QC-VECSEL architecture. Microfabrication proceeds according to the standard thermocompression bonding process described in Ref.[16] and the Supporting Information. Electrical injection occurs selectively in a central circular area by using SiO_2 to isolate surrounding waveguide regions; this encourages the lasing of the fundamental Gaussian mode in the external cavity. The ridge antennas resemble elongated microstrip patches and support a resonant mode with odd-symmetry vertical E-fields beneath the metal contact ($w \approx \lambda_0/2n$), ideal for intersubband selection rule in QC gain media. The mode profile of a single ridge is illustrated in the inset of Figure 1a. Once the material gain coefficient g exceeds the transparency gain g_{tr}, material losses are balanced, and the metasurface acts as an amplifying mirror with reflectance values above 1, as shown in Figure 1b. The peak reflectance can be approximated with an exponential model as $R_{MS}(\nu_0) \approx e^{\xi_0(g-g_{tr})}$, where ξ_0 is an effective gain interaction length at the peak value. The bandstructure of the active gain material ($GaAs/Al_{0.25}Ga_{0.75}As$) is shown in Figure 1c, which is the same as the active material used in Ref.[9].

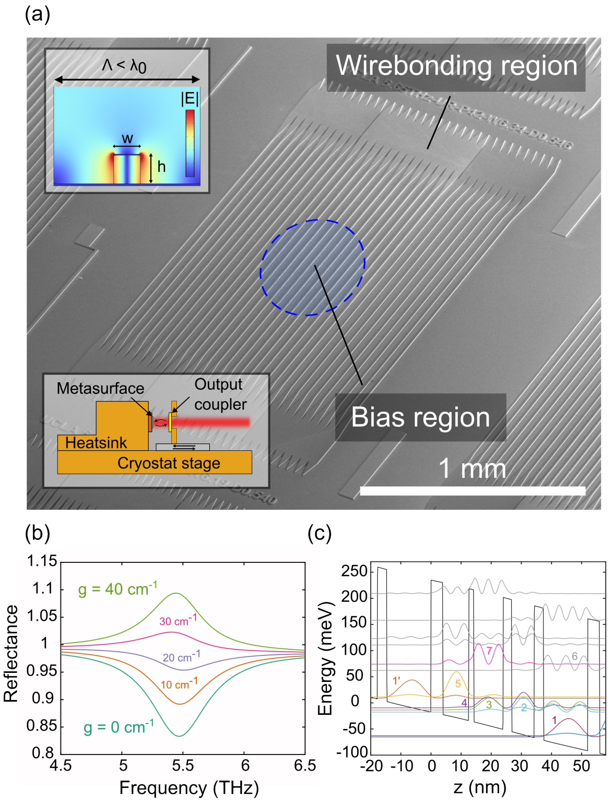

Figure 1. (a) SEM image of a representative metasurface fabricated for operation above 5 THz. The blue circle corresponds to the region of the metasurface that receives electrical injection to encourage lasing in the fundamental mode. The top inset shows the E-field mode profile and geometry of a single ridge at resonance, and the bottom inset shows a schematic of the VECSEL mount. (b) Simulated reflectance spectra of a representative metasurface with 5.45 THz resonance as a function of material gain. (c) Bandstructure and wavefunctions of the active region at 84 mV/mod. The key states are in color and labeled as 7 (parasitic), 5 (upper level), 4–2 (lower levels), and 1 (ground). The prime numbers represent the states from the previous module. The wafer number is VB1401, which is the same active region (design 2) in Ref .[9]

In principle, metasurface scaling for higher-frequency operation involves proportionally reducing structural dimensions such as period Λ, ridge width w, and height h according to wavelength. However, this scaling overlooks unfavorable trends in gain and loss.[17] Reduction of the active region thickness h leads to increased metallic cladding loss, which scales as h^{-1}. However, retaining the original thickness diminishes the metasurface's radiative quality factor, $Q_r \approx \frac{n\pi\Lambda}{8h}$,[18,19] and therefore reduces the effective gain interaction length, ξ_0, which is directly proportional to Q_r at the peak reflectance $\xi_0 = 4\Gamma v_g Q_r/\omega_0$, where v_g is the group velocity within the semiconductor, and Γ~1 is field overlap factor. As a result, $\xi_0 \approx \lambda_0\Lambda/4h$. Since the period must scale with the wavelength, if we keep the active region h constant, we see that $\xi_0 \sim \lambda_0^2$. This weakens the per-pass amplification and necessitates more reflective output couplers (OCs) to compensate for the lower round-trip gain and meet threshold conditions. While a more reflective output coupler is not inherently detrimental, for realistic devices it leads to reduced output power. This is because the efficiency of inductive mesh output couplers (ratio of the transmittance to the sum of the transmittance and absorbance) is less than unity; the absorbance from metallic losses is usually on the order of 0.4–1% which in turn limits the maximum achievable reflectance. This problem is exacerbated at higher frequencies since the metal losses worsen, which results in a further drop in optical efficiency (see Supporting Information).

Attempts to reduce the active region thickness to increase Q_r come with trade-offs. For a metasurface at 5.65 THz, simulations of the metasurface reflectance assuming periodic boundary conditions show that decreasing the thickness from 10 µm to 2 µm degrades both transparency gain and reflectance (Figure 2), as the increase in ξ_0 is overtaken by rising metallic loss. Although Figure 2 shows no particular drawback for using a thick active region, further simulations based upon finite boundary conditions reveal that thicker active regions increase coupling to lossy surface Bragg modes. Therefore, a thickness of 7 µm is chosen (dashed red line)—slightly above the wavelength-scaled value from the best performing QC-VECSELs at 3.4 THz[12]—to avoid excessive metallic losses.

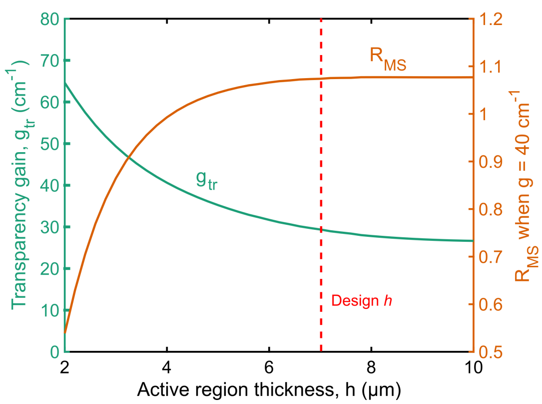

Figure 2. Transparency gain and peak metasurface reflectance versus active region thickness, for metasurface with nominal design frequency of 5.65 THz and 36 μm period. The dashed red line shows the selected active region thickness (7 μm), which aims at minimizing the transparency gain while avoiding overly thick active regions which would result in excessively low Q_r and increased coupling to lossy modes.

As the metasurface period approaches the free-space wavelength $\Lambda \approx \lambda_0$, the localized metasurface resonances hybridize with a surface-wave mode that propagates along the metasurface at grazing incidence. First order Bragg scattering from the grating further couples this mode to normally incident/emitted radiation. This can be seen in Figure 3a, where a plot of various modal eigenfrequencies mapping of an infinite uniform metasurface vs. period reveals a characteristic anticrossing between the desired metasurface mode (green curve) and the surface-wave “Bragg” mode (orange curve). In a finite sized metasurface, this constitutes a loss mechanism, since these propagating modes can “escape” the bias region, into the unbiased/lossy region, or even off the metasurface entirely. The lower the radiative quality factor Q_r, the larger the magnitude of the splitting; to avoid this enhanced coupling, one must keep the period Λ even smaller.

To quantify this phenomenon, a cavity eigenmode simulation is performed on a finite-sized metasurface where only the 0.5-mm-diameter central region is biased to provide gain, and the rest of the unbiased metasurface is lossy. The threshold gain g_{th} – i.e. the amount of material gain required to balance losses – is simulated for metasurfaces with 5 μm and 7 μm thick active regions in a 1-mm-long external cavity. As shown in Figure 3b, increasing the period initially leads to modest improvements in reflectance and a gradual decrease in threshold gain. However, beyond a critical period (~40 μm), coupling to the surface-propagating Bragg mode becomes dominant, causing the threshold gain to rise sharply. This rise occurs at different critical periods for the two thicknesses, indicating that the coupling strength to these parasitic modes is dependent on the active region thickness and radiative quality factor of the metasurface. The natural conclusion is that the period should be kept small: $\Lambda < 0.7\ \lambda_0$.

However, reducing the period also has consequences. Simply scaling the period from the 3.4 THz design[12] (Λ: 41.7 μm → 26 μm) reduces ξ_0, which is not tolerable due to the increased losses and small available gain above 5 THz. While output couplers with higher reflectance could, in principle, compensate for this, they reduce optical efficiency and power output. Moreover, they do not mitigate diffraction losses from external cavity imperfections. Another complication with reducing the period is the possibility of self-lasing, which occurs when the metasurface supports a sufficiently high-quality factor mode that lases without an external cavity (i.e., without an output coupler). While self-lasing of the propagating fundamental ridge mode is effectively suppressed due to its very high threshold (dashed green line), the surface-confined dark mode (yellow curve) at the Brillouin zone boundary ($k_x = \pi/\Lambda$) under periodic boundary conditions can still self-lase. This dark mode is an antisymmetric supermode in which adjacent ridges oscillate out of phase (see Supporting Information). For $\Lambda < 0.5\ \lambda_0$, it cannot couple to propagating free-space radiation, becoming non-radiative or "dark" with a large quality factor. Consequently, it has a relatively low self-lasing threshold (dashed yellow curve) and competes with the desired symmetric metasurface supermode. To suppress this competing dark mode, the period should remain above 0.5λ₀. For Λ > 0.5λ₀, radiative losses increase sharply, preventing self-lasing, and the dark mode shifts to lower frequencies outside the gain bandwidth due to anti-crossing with a corresponding antisymmetric Bragg mode (purple curve).

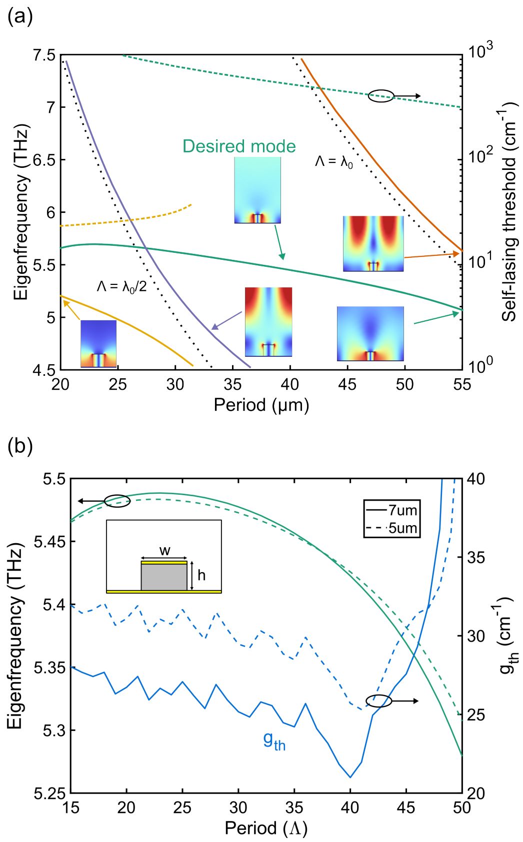

Figure 3. (a) Eigenfrequency vs. period from FEM simulations for four eigenmodes of an infinite uniform ridge metasurface. Dashed lines indicate self-lasing thresholds of the corresponding metasurface mode whose eigenfrequency is plotted in solid line of matching color. The green line marks the target metasurface mode, the orange line shows a coupled surface-propagating mode, the yellow line represents the anti-symmetric dark mode, and the purple line shows the anti-symmetric Bragg mode. The dotted black lines represent the calculated frequency of the first order and anti-symmetric Bragg modes ($\nu_1 = c/\Lambda$ and $\nu_2 = c/2\Lambda$, respectively) (b) FEM results for a finite-size VECSEL at h=7 μm and h=5 μm. Eigenfrequency and threshold gain are plotted versus period. Simulation parameters: w=6.72 µm, d=0.5 mm, and L=1.0 mm.

In essence, the choice of period is not only constrained by metasurface resonance requirements but also by the need to avoid diffraction-mediated loss channels that emerge from surface modes. The coupling strength between the desired lasing mode and surface-propagating modes increases as the Q_r decreases, and energy that would otherwise be reflected coherently is instead dissipated at the metasurface boundaries. These findings emphasize that metasurface design at frequencies above 5 THz requires not just geometric scaling, but also careful optimization of thickness, periodicity, and output coupling to mitigate the compounded effects of reduced reflectance, increased loss, and modal hybridization.

RESULTS AND DISCUSSION:

Metasurfaces with varying periods (Gen1: Λ = 36–44 μm, Gen2: Λ = 24–32 μm) were fabricated using the QC active region described in Ref.[9] (wafer number VB1401). The metasurfaces were mounted with output couplers to create plano-plano VECSEL cavities with cavity lengths tunable roughly from 0.1–1 mm with an intracryostat piezoelectric stepper. Table 1 summarizes the key parameters and characterization results.

Table 1. Summary of design parameters and characterization results for Gen1 and Gen2 devices.

Device	**Design (THz); Type**	***w*/*h*/*Λ* (μm)**	**Bias Ø (mm)**	**Tuning Range (THz) @ *T***	**Pulsed Peak Power @ *T***	**Pulsed T_{max}**	**CW Operation**	**R_{OC}**
0923BR (Gen1)	5.45; Uniform	6.72/7/40	0.520	N/A	N/A	No lasing	No (>5 K)	>0.99 (OC3)
0923FR (Gen1)	5.65; Uniform	6.53/7/36	0.540	5.40–5.72 (~320 GHz) @ 5 K	66 μW @ 5 K	50 K	No (>5 K)	0.99 (OC1)
0923FL (Gen1)	5.45; Uniform	6.81/7/36	0.540	5.35–5.60 (~250 GHz) @ 5 K	1.3 mW @ 5 K	47 K	No (>5 K)	0.976–0.983 (OC2)
0325CL (Gen2)	5.45; Focusing	6.68–6.91/7/32	0.416	5.27–5.69 (~417 GHz) @ 41 K	1 mW @ 41 K	70 K	Yes (T_{max} ~42 K)	0.99 (OC1)

Device	Design (THz); Type	$w/h/\Lambda$ (μm)	Bias Ø (mm)	Tuning Range (THz) @ T	Pulsed Peak Power @ T	Pulsed T_{max}	CW Operation	R_{OC}
Same as above	*Same*	*Same*	*Same*	5.23–5.73 (~500 GHz) @ 41 K	87 μW @ 41 K	78 K	Yes (T_{max} ~54 K)	>0.99 (OC3)
0325DL (Gen2)	5.65; Focusing	6.22–6.64/7/30	0.39	5.33–5.74 (~410 GHz) @ 41 K	0.25 mW @ 41 K	80 K	Yes (T_{max} ~ 51 K)	0.99 (OC1)
0325DR (Gen2)	*Same*	*Same*	0.510	N/A (Fixed cavity)	1 mW @ 41 K	83 K	No (>40 K)	0.99 (OC1)

First-generation (Gen1) devices featured uniform-ridge metasurfaces with Λ = 36 and 40 μm. In general, the performance of these devices was disappointing. Only the Λ = 36 μm devices (0923FR and 0923FL) lased, and only in pulsed mode; larger-period devices did not lase at all. We attribute this poor performance to the aforementioned increased loss from coupling to surface Bragg modes (see Methods). Device 0923FR (designed at 5.65 THz, using OC1) achieved a tuning bandwidth of ~320 GHz (5.8% fractional) and a pulsed T_{max} of 50 K. Reducing the nominal resonant frequency to 5.45 THz (device 0923FL) and switching to the less reflective OC2 increased peak output power to 1.3 mW at 5 K, though the tuning bandwidth dropped to ~250 GHz. The T_{max} remained similar (~47 K), indicating reduced coupling to lossy modes. Neither Gen1 device achieved CW operation.

Following a detailed simulation campaign (the results of which are summarized in Figure 3), a second-generation (Gen2) of metasurface devices were redesigned and fabricated with reduced periods ($\Lambda <$ 32 μm) with the intention of avoiding coupling to the surface Bragg modes. Furthermore, we employed a focusing metasurface design in which the ridge widths are spatially modulated to impose a parabolic reflection phase with a 2.5 mm focal length.[20] For the short cavity lengths employed ($L_c \sim 0.1$ mm), the focusing effect likely had little benefit on the beam; perhaps the greater benefit was that breaking ridge-width uniformity disrupted coupling to Bragg modes.

Significant improvements in performance were achieved with the Gen2 metasurfaces compared with Gen1. Device 0325CL (designed at 5.45 THz, Λ = 32 μm) using OC1 achieved 1 mW peak power and lased up to 70 K (Figure 4b) and ~417 GHz tuning bandwidth (7.6% fractional) at 41 K. With the higher reflectance OC3, tuning bandwidth was increased to ~500 GHz (9.1% fractional) at 41 K (Figure 4a). As the piezo stage is stepped out and cavity length gets larger, the laser frequency red-shifted from 5.73–5.23 THz, until the lasing mode fell outside the range with enough gain (i.e, $g < g_{th}$) and lasing stopped for 8 cavity steps (~ 3.2 μm), after which lasing started again in the next longitudinal mode $m_0 + 1$. We describe this as "gain-bandwidth-limited" tuning operation. As the cavity length gets larger, the tuning range reduces while still being gain-bandwidth limited (not FSR-induced mode hopping). Therefore, the available gain-bandwidth is getting smaller as the external cavity gets larger, which is due to increased diffraction losses and a changing transverse confinement factor. The loss from using the higher reflectance output coupler

OC3 also enabled CW operation with 23 μW power (corrected for cooler window transmission), $T_{\max}$ of 54 K and tuning bandwidth of ~278 GHz (5% fractional; see Figure 4c).

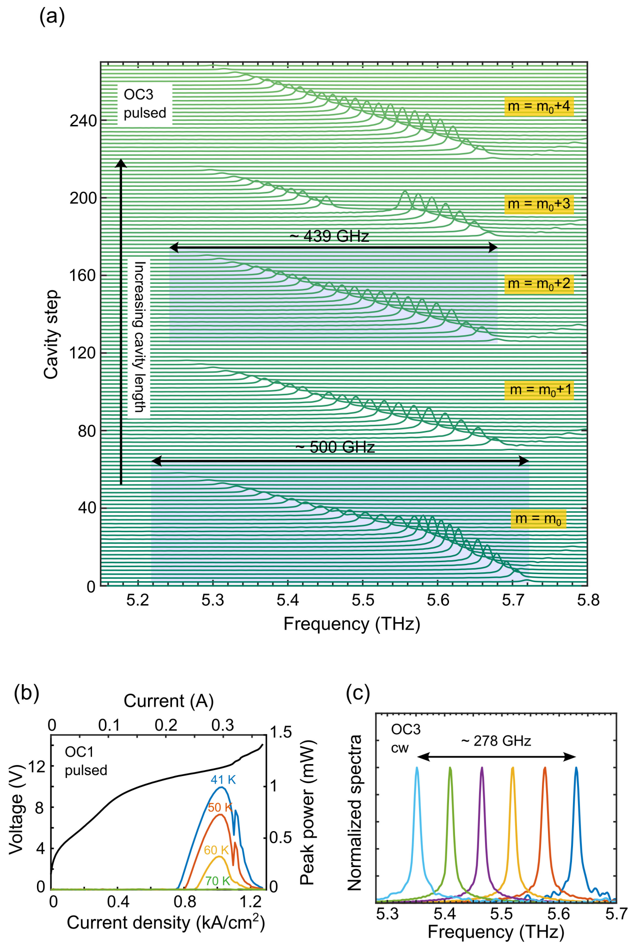

Figure 4. (a) Emission spectra of 0325CL with OC3 as the cavity length is increased. (b) Light-current-voltage of 0325CL with OC1 (99% reflectance). Peak power is corrected for 67% transmission through the 2 mm-thick HDPE window. (c) CW spectra of 0325CL using OC3 (>99% reflectance).

Another set of focusing devices designed at 5.65 THz with Λ = 30 μm was tested using OC1 to investigate the beam quality and trends in the threshold current density and slope efficiency. Device 0325DL achieved 0.25 mW peak power and ~410 GHz tuning bandwidth at 41 K. A circular beam pattern is maintained across the whole tuning range, as shown in Figure 5a. The extracted threshold current density J_{th} and slope efficiencies η_s are plotted as the cavity is stepped (Figure 5b). Although device 0325DL was designed for 5.65 THz, the lowest threshold current density occurred at 5.51 THz which is most likely due to the increased phonon losses in GaAs at higher frequencies. At lower frequencies, the threshold rose again as the laser moved away from designed frequency. Slope efficiency is maximized around 5.45 THz, which is around 5 mW/A. The reason for the increase in slope efficiency off-resonance is primarily due to the increase in optical efficiency η_{opt} which results from a reduction in ξ as ν is detuned from ν_0.[17] The variations in output coupler reflectance likely play a role in these trends as well, though difficult to confirm due to low SNR in the transmission measurement.

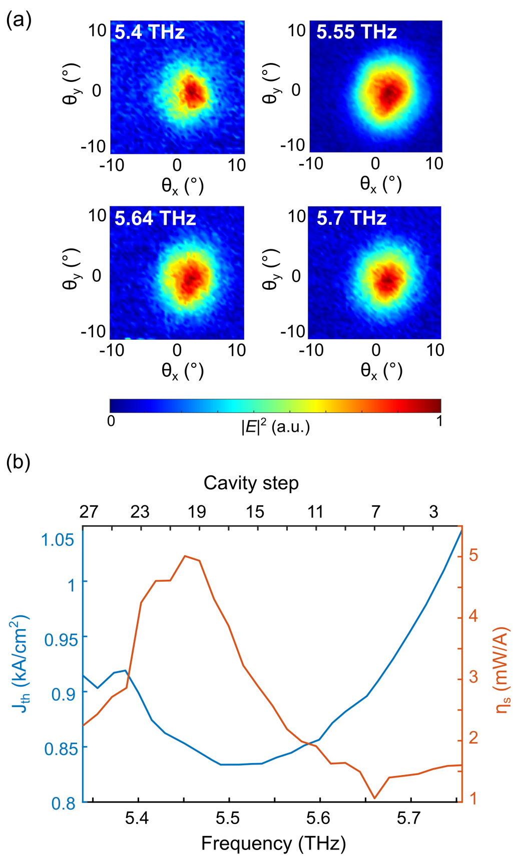

Figure 5. Device 0325DL with OC1: (a) Laser beam-pattern for various cavity positions and frequencies. (b) Measured laser threshold current density and slope efficiency at 41 K as a function of cavity step and frequency.

Finite metasurface simulations of the focusing design (Device 0325DL) were conducted to investigate the frequency dependence of threshold current density shown in Figure 5. Assuming a homogeneously broadened gain medium, and spectrally flat material gain and output coupler reflectance, variations in threshold current density are attributed primarily to changes in threshold gain and GaAs dispersion. While both the material gain and output coupler reflectance are in fact not spectrally flat, this assumption helps to isolate the effect of the GaAs dispersion. The simulated mode profile (Figure 6a) for a 1.75 λ_0 cavity shows that, unlike a uniform metasurface, the focusing design confines the fundamental mode within the bias diameter, with intensity dropping rapidly and reducing field uniformity. The extracted threshold gain (g_{th}) matches the trend of the measured J_{th} (Figure 6c), with a maximum field confinement factor in the bias area near 5.68 THz and a g_{th} minimum at 5.41 THz (solid blue line). When phonon losses are excluded, the g_{th} minimum shifts to ~5.78 THz (dashed blue line), confirming the effect of GaAs dispersion in g_{th} minimum which can be detuned from the metasurface designed frequency.

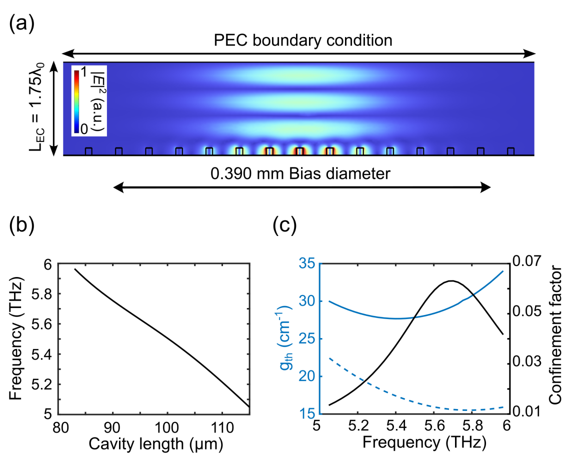

Figure 6. (a) FEM simulation of the finite focusing metasurface (Device 0325DL) using a PEC boundary condition instead of an output coupler. (b) Frequency of the fundamental mode as a function of cavity length. (c) Extracted threshold gain and bias region confinement factor as the cavity length is stepped. The solid blue line is the case of including all waveguide losses (metal and phonon), while the dashed blue line corresponds to removing the phonon losses from the simulation. Bias region field confinement factor is the ratio of the y-component of the E-field in the biased ridges to the entire E-field in all domains.

To understand the performance limitations of the QC-VECSELs in this work and suggest a path forward, we analyze its wall plug efficiency (WPE) relative to a benchmark metal-metal (MM) waveguide laser fabricated from the same active region.[9] We focus on the highest WPE QC-VECSEL device in this work (Device 0325CL with OC1). At 41 K it exhibits a maximum WPE of 0.028% (approximately 8× lower than the MM waveguide (0.23%)), and a slope efficiency of 17 mW/A (approximately 2.5× lower than the MM waveguide (42 mW/A)).

A simple expression for WPE is given by:

$$WPE = \frac{N_p h\nu}{eV}\eta_i \eta_{opt} \eta_u \frac{I - I_{th}}{I},$$

where the prefactor corresponds to the voltage efficiency (η_V), and the final factor represents current efficiency (η_I). Since both devices share the same active region and wire bonding configuration (to the ground plane), we assume similar internal quantum efficiency ($\eta_i \approx 0.12$) and voltage efficiency ($\eta_V \approx 0.24$). The η_i is calculated from the slope efficiency of the MM waveguide by assuming $\eta_{opt} \approx 0.12$ from simulated waveguide and mirror losses[9]. The reduced WPE in the QC-VECSEL must therefore arise from three factors. First, *modal uniformity* (η_u) is ~1.5× smaller in the QC-VECSEL compared to the MM waveguide. A MM waveguide cavity lasing in multiple longitudinal modes more uniformly saturates the gain along its length, in contrast to the non-uniform electric field in the ridge antennas of the metasurface. Second, the measured *current efficiency* (η_I) for the QC-VECSEL is $\eta_I \approx 0.26$, about 2.5× lower than the MM waveguide's ($\eta_I \approx 0.66$), due to increased losses that raise the threshold current (see Methods). Finally, from the slope efficiency, an optical efficiency (η_{opt}) of ~0.074 for the QC-VECSEL is calculated, about 1.6× lower than the MM waveguide's (simulated value ~0.12). This is the most striking, since at lower frequencies the QC-VECSEL usually has a much higher

η_{opt} value than the MM waveguide. The fact that this number is so low indicates that there is still considerable loss associated with the VECSEL cavity and metasurface. This is exacerbated by the need for high-reflectance output couplers to overcome high threshold gain which in turn reduces the output coupling efficiency ($\eta_{OC} \approx 28\%$ at 5.38 THz). The product of these individual contributions (~6.2×) falls short of the measured WPE ratio (~8×), which we attribute to factors like output power roll-off, non-uniform field intensity across the biased ridges in the focusing QC-VECSEL, and the uncertainties in the simulated optical efficiency of the MM waveguide.

These results show that the priority for high-frequency QC-VECSELs must be to reduce excess losses. Steps towards achieving this goal include optimizing the cavity design and selecting an appropriate output coupler. Promising approaches include implementing off-axis parabolic (OAP) mirror-based cavities to lower diffraction losses. This has been shown to improve operating temperatures in both pulsed and CW mode compared to QC-VECSELs with identical active regions but plano–plano cavities and larger bias diameters.[21] However, this would only work for a uniform, not focusing, metasurface design. Additionally, the output coupler efficiency drops rapidly with increasing reflectance due to the metallic losses (see Supporting Information). This results in overall lower power output and slope efficiency. Therefore, switching to an all-dielectric output coupler will have a significant impact on optical efficiency at these high frequencies – we estimate > 3x improvement in slope efficiency. Together, the aforementioned steps could further boost device performance and improve slope efficiency, output power, and T_{max}, and further enhance CW performance.

CONCLUSION:

In summary, QC-VECSELs operating above 5 THz were studied via electromagnetic simulations, revealing deviations from conventional periodicity rules and key trade-offs between threshold gain and efficiency. Both uniform-ridge and focusing metasurfaces with varying periods were fabricated and characterized, showing improved performance with decreasing period ($\Lambda < 0.7\ \lambda_0$). By employing output couplers with reflectance from 0.97 to >0.99, we demonstrated pulsed operation up to 5.74 THz with peak powers of 1.3 mW, T_{max} of 83 K, and CW operation up to 54 K. Additionally, we achieved ~500 GHz of frequency tunability (~9.1% fractional tuning) and Gaussian far-field profiles across the entire range, underscoring their potential as LOs for advanced heterodyne spectrometers.

ASSOCIATED CONTENT

Supporting Information

Metasurface fabrication process details, quartz output coupler designs and their corresponding reflectance and efficiency simulations, self-lasing mechanisms of the metasurface with supporting simulations.

AUTHOR INFORMATION

Corresponding Author

Mohammad Shahili − Department of Electrical and Computer Engineering, University of California, Los Angeles, CA 90095, USA, E-mail: mshahili0@g.ucla.edu. https://orcid.org/0000-00027103-3876

Author Contributions

The manuscript was written through contributions of all authors. All authors have given approval to the final version of the manuscript. ‡Mohammad Shahili and Anthony D. Kim contributed equally to this work.

Funding Sources

Funding was provided by the National Aeronautics and Space Administration (80NSSC22K1894).

ACKNOWLEDGMENT

The fabrication was carried out in part at the University of California Santa Barbara, Nanofabrication Facility, and the University of California Los Angeles, Nanofabrication Laboratory. This work was performed, in part, at the Center for Integrated Nanotechnologies, an Office of Science User Facility operated for the U.S. Department of Energy (DOE) Office of Science. Sandia National Laboratories is a multimission laboratory managed and operated by National Technology and Engineering Solution of Sandia, LLC, a wholly owned subsidiary of Honeywell International, Inc., for the U.S. Department of Energy's National Nuclear Security Administration under contract DE-NA-0003525.

REFERENCES

(1) Goldsmith, P. F. Sub-Millimeter Heterodyne Focal-Plane Arrays for High-Resolution Astronomical Spectroscopy. *URSI Radio Sci. Bull.* **2017**, *2017* (362), 53–73. https://doi.org/10.23919/URSIRSB.2017.8267373.

(2) Richter, H.; Wienold, M.; Schrottke, L.; Biermann, K.; Grahn, H. T.; Hübers, H.-W. 4.7-THz Local Oscillator for the GREAT Heterodyne Spectrometer on SOFIA. *IEEE Trans. THz Sci. Technol.* **2015**, *5* (4), 539–545. https://doi.org/10.1109/TTHZ.2015.2442155.

(3) Khalatpour, A.; Paulsen, A. K.; Addamane, S. J.; Deimert, C.; Reno, J. L.; Wasilewski, Z. R.; Hu, Q. A Tunable Unidirectional Source for GUSTO's Local Oscillator at 4.74 THz. *IEEE Trans. THz Sci. Technol.* **2022**, *12* (2), 144–150. https://doi.org/10.1109/TTHZ.2021.3124310.

(4) Wienold, M.; Semenov, A. D.; Dietz, E.; Frohmann, S.; Dern, P.; Lü, X.; Schrottke, L.; Biermann, K.; Klein, B.; Hübers, H.-W. OSAS-B: A Balloon-Borne Terahertz Spectrometer

for Atomic Oxygen in the Upper Atmosphere. *IEEE Trans. THz Sci. Technol.* **2024**, *14* (3), 327–335. https://doi.org/10.1109/TTHZ.2024.3363135.
(5) Peeters, E.; Martín-Hernández, N. L.; Damour, F.; Cox, P.; Roelfsema, P. R.; Baluteau, J.-P.; Tielens, A. G. G. M.; Churchwell, E.; Kessler, M. F.; Mathis, J. S.; Morisset, C.; Schaerer, D. ISO Spectroscopy of Compact HII Regions in the Galaxy: I. The Catalogue. *A&A* **2002**, *381* (2), 571–605. https://doi.org/10.1051/0004-6361:20011516.
(6) Wienold, M.; Röben, B.; Lü, X.; Rozas, G.; Schrottke, L.; Biermann, K.; Grahn, H. T. Frequency Dependence of the Maximum Operating Temperature for Quantum-Cascade Lasers up to 5.4 THz. *Applied Physics Letters* **2015**, *107* (20), 202101. https://doi.org/10.1063/1.4935942.
(7) Moore, W. J.; Holm, R. T. Infrared Dielectric Constant of Gallium Arsenide. *Journal of Applied Physics* **1996**, *80* (12), 6939–6942. https://doi.org/10.1063/1.363818.
(8) Li, W.; Ma, Y.; Xu, Y.; Liu, J.; Wang, L.; Zhuo, N.; Lu, Q.; Zhang, J.; Zhai, S.; Liu, S.; Liu, F. Continuous-Wave Single-Mode Quantum Cascade Laser at 5.1 THz Based on Graded Sampled Grating Design. *Photon. Res.* **2022**, *10* (12), 2686. https://doi.org/10.1364/PRJ.467974.
(9) Shahili, M.; Addamane, S. J.; Kim, A. D.; Curwen, C. A.; Kawamura, J. H.; Williams, B. S. Continuous-Wave GaAs/AlGaAs Quantum Cascade Laser at 5.7 THz. *Nanophotonics* **2024**, *0* (0). https://doi.org/10.1515/nanoph-2023-0726.
(10) Xu, L.; Curwen, C. A.; Hon, P. W. C.; Chen, Q.-S.; Itoh, T.; Williams, B. S. Metasurface External Cavity Laser. *Applied Physics Letters* **2015**, *107* (22), 221105. https://doi.org/10.1063/1.4936887.
(11) Curwen, C. A.; Reno, J. L.; Williams, B. S. Terahertz Quantum Cascade VECSEL with Watt-Level Output Power. *Applied Physics Letters* **2018**, *113* (1), 011104. https://doi.org/10.1063/1.5033910.
(12) Curwen, C. A.; Reno, J. L.; Williams, B. S. Broadband Continuous Single-Mode Tuning of a Short-Cavity Quantum-Cascade VECSEL. *Nat. Photonics* **2019**, *13* (12), 855–859. https://doi.org/10.1038/s41566-019-0518-z.
(13) Curwen, C. A.; Kawamura, J. H.; Hayton, D. J.; Addamane, S. J.; Reno, J. L.; Williams, B. S.; Karasik, B. S. Phase Locking of a THz QC-VECSEL to a Microwave Reference. *IEEE Trans. THz Sci. Technol.* **2023**, *13* (5), 448–453. https://doi.org/10.1109/TTHZ.2023.3280451.
(14) Wu, Y.; Curwen, C. A.; Shahili, M.; Reno, J. L.; Williams, B. S. RF Injection Locking of THz Metasurface Quantum-Cascade VECSEL. *Laser & Photonics Reviews* **2023**, *17* (8), 2300007. https://doi.org/10.1002/lpor.202300007.
(15) Curwen, C. A.; Kim, A. D.; Karasik, B. S.; Kawamura, J. H.; Williams, B. S. Optical Injection Locking of a THz Quantum-Cascade VECSEL with an Electronic Source. *Opt. Lett.* **2023**, *48* (14), 3809. https://doi.org/10.1364/OL.492182.
(16) Williams, B. S.; Kumar, S.; Hu, Q.; Reno, J. L. Operation of Terahertz Quantum-Cascade Lasers at 164 K in Pulsed Mode and at 117 K in Continuous-Wave Mode. *Opt. Express* **2005**, *13* (9), 3331. https://doi.org/10.1364/OPEX.13.003331.
(17) Kim, A. D.; Curwen, C. A.; Wu, Y.; Reno, J. L.; Addamane, S. J.; Williams, B. S. Wavelength Scaling of Widely-Tunable Terahertz Quantum-Cascade Metasurface Lasers. *IEEE J. Microw.* **2023**, *3* (1), 305–318. https://doi.org/10.1109/JMW.2022.3224640.

(18) Hon, P. W. C.; Tavallaee, A. A.; Chen, Q.-S.; Williams, B. S.; Itoh, T. Radiation Model for Terahertz Transmission-Line Metamaterial Quantum-Cascade Lasers. *IEEE Trans. THz Sci. Technol.* **2012**, *2* (3), 323–332. https://doi.org/10.1109/TTHZ.2012.2191023.
(19) Hon, P. W. C.; Liu, Z.; Itoh, T.; Williams, B. S. Leaky and Bound Modes in Terahertz Metasurfaces Made of Transmission-Line Metamaterials. *Journal of Applied Physics* **2013**, *113* (3), 033105. https://doi.org/10.1063/1.4776761.
(20) Xu, L.; Chen, D.; Itoh, T.; Reno, J. L.; Williams, B. S. Focusing Metasurface Quantum-Cascade Laser with a near Diffraction-Limited Beam. *Opt. Express* **2016**, *24* (21), 24117. https://doi.org/10.1364/OE.24.024117.
(21) Wu, Y.; Curwen, C. A.; Hayton, D. J.; Reno, J. L.; Williams, B. S. Continuous Wave Operation of Terahertz Metasurface Quantum-Cascade VECSEL with a Long Intra-Cryostat Cavity. *Applied Physics Letters* **2022**, *121* (19), 191106. https://doi.org/10.1063/5.0107667.

For Table of Content Use Only

Manuscript title: Tunable metasurface external-cavity quantum cascade lasers up to 5.74 THz

Authors: Mohammad Shahili, Anthony D. Kim, Sadhvikas J. Addamane, Christopher A. Curwen, Jonathan H. Kawamura, Benjamin S. Williams

Synopsis for graphic: The graphic is from Figure 1 in the manuscript. It shows a representative SEM of the metasurface demonstrated in this paper.